Spatial distribution and activity of Na +/K +-ATPase in lipid bilayer membranes with phase boundaries

Bhartia, Tripta; Cornelius, Flemming; Brewer, Jonathan R.; Bagatolli, Luis; Simonsen, Adam Cohen; Ipsen, John Hjort; Mouritsen, Ole G.

Published in:
Biochimica et Biophysica Acta. Biomembranes

DOI:
10.1016/j.bbamem.2016.03.015

Publication date:
2016

Document version
Peer reviewed version

Biochimica et Biophysica Acta 1858 (2016) 1390–1399

Contents lists available at ScienceDirect

Biochimica et Biophysica Acta

journal homepage: www.elsevier.com/locate/bbamem

Spatial distribution and activity of Na $^{+}$/K $^{+}$-ATPase in lipid bilayer membranes with phase boundaries

Tripta Bhatia [a,b,e,*], Flemming Cornelius [d], Jonathan Brewer [a,c], Luis A. Bagatolli [a,c], Adam C. Simonsen [a,b], John H. Ipsen [a,b], Ole G. Mouritsen [a,b]

[a] MEMPHYS — Center for Biomembrane Physics, University of Southern Denmark, DK-5230 Odense M, Denmark
[b] Department of Physics, Chemistry, and Pharmacy, University of Southern Denmark, DK-5230 Odense M, Denmark
[c] Department of Biochemistry and Molecular Biology, University of Southern Denmark, DK-5230 Odense M, Denmark
[d] Department of Biomedicine, Aarhus University, DK-8000 Aarhus C, Denmark
[e] Max Planck Institute of Colloids and Interfaces, Department of Theory and Bio-Systems, Science Park Golm, 14476 Potsdam, Germany

ARTICLE INFO

Article history:
Received 26 December 2015
Received in revised form 20 February 2016
Accepted 10 March 2016
Available online 16 March 2016

Keywords:
Membranes
Na $^{+}$/K $^{+}$-ATPase
Giant unilamellar vesicles
Domains
Membrane protein
Protein–lipid interaction
Membrane biophysics

ABSTRACT

We have reconstituted functional Na $^{+}$/K $^{+}$-ATPase (NKA) into giant unilamellar vesicles (GUVs) of well-defined binary and ternary lipid composition including cholesterol. The activity of the membrane system can be turned on and off by ATP. The hydrolytic activity of NKA is found to depend on membrane phase, and the water relaxation in the membrane on the presence of NKA. By collapsing and fixating the GUVs onto a solid support and using high-resolution atomic-force microscopy (AFM) imaging we determine the protein orientation and spatial distribution at the single-molecule level and find that NKA is preferentially located at l_o/l_d interfaces in two-phase GUVs and homogeneously distributed in single-phase GUVs. When turned active, the membrane is found to unbind from the support suggesting that the protein function leads to softening of the membrane.

1. Introduction

For more than three decades it has been hypothesized that the meso-scale lateral organization of biological membranes is an important factor for membrane-protein interactions [1]. The lipid rafts hypothesis proposes that specialized lipid nanodomains, termed rafts, that are rich in saturated lipid chains and cholesterol form platforms for protein sorting and function [2,3,4,5,6,7]. Interestingly, from a purely membrane biophysics perspective, lipid membranes with and without proteins do show lipid-mediated lateral heterogeneity [8,9,10,11,12]. We have earlier imaged small domains of size ≈100 nm deep inside the liquid ordered (l_o)–liquid disordered (l_d) coexistence region [13], which are spontaneously generated due to low line tension ≈1 pN [12]. The domains are considered to be pseudo-critical fluctuations and are detected in the one-component saturated and mono-saturated lipid monolayers and bilayers near the main phase transition and in the ternary lipid mixture over a wide range of compositions [8,9,10,11,12,13]. These domains are suggested to provide a mechanism for lipid aggregation and stabilization of lipid–protein complexes, away from phase coexistence [14], and have major influence on bilayer mechanics and permeability [15,16]. In the present work we analyze the lateral structure of well-defined model membranes at mesoscopic and nanoscopic length scales using giant unilamellar vesicles (GUVs) composed of two or three lipid components, i.e., DOPC-chol and DOPC–DPPC-chol, containing Na $^{+}$/K $^{+}$-ATPase (NKA), a trans-membrane (TM) protein suggested to be associated with specialized domains rafts [17,18]. NKA hydrolyzes adenosine triphosphate (ATP) and uses the free energy of hydrolysis for maintaining the TM Na $^{+}$ and K $^{+}$ ions-gradients across cell membranes. The kinetics of ions transport is described by Albers–Post reaction cycle or E_1–E_2 model, where E_1 and E_2 are the two conformations of the NKA in the lipid-bilayer with high Na $^{+}$ and high K $^{+}$ affinities respectively [19,20]. The two main sub-units of the NKA are an α-subunit (containing the catalytic residues, ion occlusion, transport pathways, and inhibitor binding sites) with 10 TM segments and a single TM glycosylated β-subunit (important for protein folding, trafficking to the plasma membrane, stabilization, K-occlusion, and cell-adhesion) as shown in Fig. 1a. The bilayer can adjust in the vicinity of NKA by stretching/compressing and bending of lipids in order to match the TM hydrophobic thickness as shown in Fig. 1a. A third small, regulatory protein called FXYD is also associated. The cross sectional area of NKA varies from cytoplasmic (cyt) to extracellular (ext) side and with the conformation and is approx 12.6 nm^2 in E_1-conformation near the ext

* Corresponding author at: Max Planck Institute of Colloids and Interfaces, Department of Theory and Bio-Systems, Science Park Golm, 14476 Potsdam, Germany.
E-mail address: Tripta.Bhatia@mpikg.mpg.de (T. Bhatia).

http://dx.doi.org/10.1016/j.bbamem.2016.03.015
0005-2736/

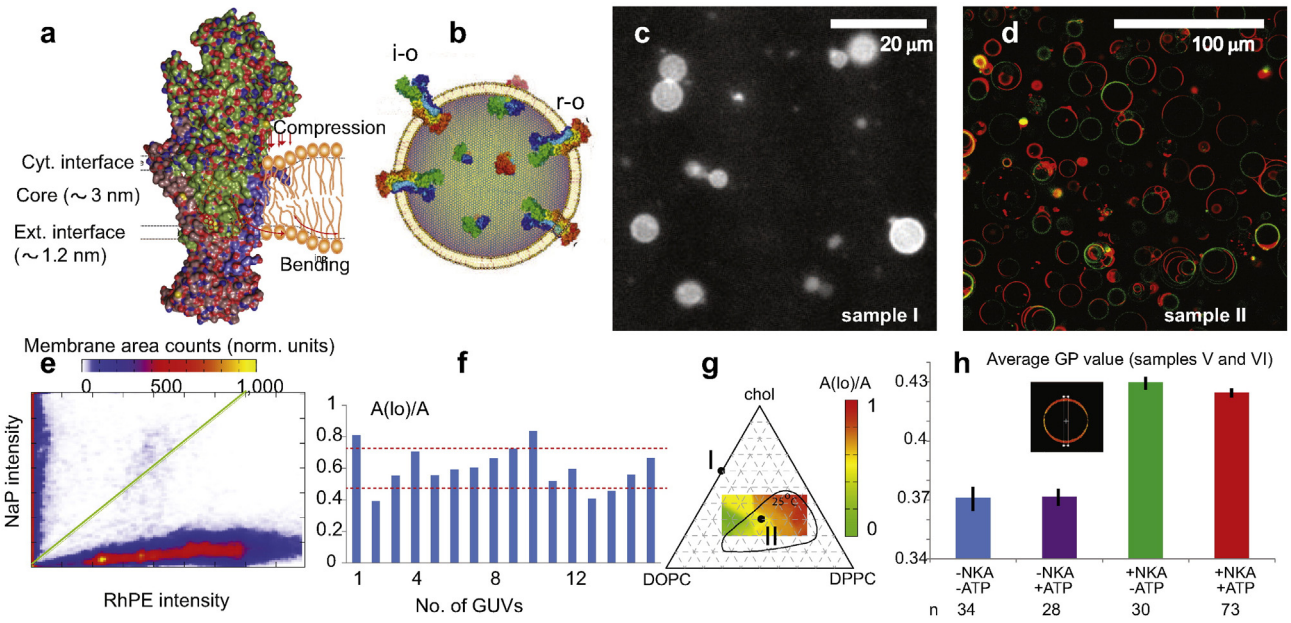

Fig. 1. NKA graphical illustration, GUVs of two- and three-component lipid mixtures, area fractions of separated phases, orientation of NKA in vesicles, and GP measurements. (a) A cartoon showing the membrane deformation adjacent to the protein and the NKA subunits: α-subunit (green), β-subunit (raspberry) and FXYD-subunit (blue). Cytoplasmic (cyt) to extracellular (ext) sides are shown (reproduced from [21]). (b) A graphical illustration of the orientations of NKA in a proteoliposome (taken from [19]). Rightside-out (r-o) is the native membrane configuration and inside-out (i-o) is opposite of the r-o orientation. A third orientation non-oriented (n-o) is not shown. (c) Epi-fluorescence image of GUVs (sample I) and (d) confocal-fluorescence image of GUVs (sample II) containing NKA settled at the bottom in an observation chamber. In ternary GUVs, the two fluorescence dyes NaP (green) and RhPE (red) are known to preferentially partition into the l_o and l_d phases, respectively. (e) A typical 2D-histogram of the fluorescence intensities of NaP and RhPE on an arbitrary vesicle surface. The green line is the threshold used to distinguish between l_o and l_d membrane domains. (f) The area-fraction of the l_o phase $A(l_o)/A$ is plotted for the 16 random GUVs (for sample II) analyzed. The standard deviation ($\pm$10.2%) is indicated by the gap between the two red-dashed lines. (g) Phase-diagram of the ternary lipid mixture displaying liquid–liquid coexistence region at 25°C, adapted from [35]. The black dots represent samples I and II. The color map display the $A(l_o)/A$ measured in GUVs prepared by dissolving lipids in organic solvent (taken from [36]). (h) The average GP value measured before and after adding ATP (to a final concentration of 2 mM) in samples V and VI, with error bars displaying standard error on the mean (SEM). The different measurements are shown by different colors; blue for GUVs, violet for GUVs with ATP added, green for GUVs containing NKA but, no ATP added and red for GUVs containing NKA with ATP added. In the inset, a selected GUV in the l_o membrane phase (sample V) displaying the Laurdan GP image at the equatorial region is shown. The white box is where the fluorescence counts for the GP are measured.

interphase [21]. From the crystal structures of NKA in the E_2-P and E_1~P.ADP conformations the cyt and ext protrusions from the membrane faces are approximately 4 nm and 8 nm [22,23]. Fig. 1b shows the possible orientations of the reconstituted NKA in the proteoliposomes: rightside-out (r-o) which is the native membrane configuration, inside-out (i-o) is the opposite of r-o orientation, and a third orientation non-oriented (n-o) has both sides exposed to the medium (not shown) [19,24,22,23]. NKA accounts for about 25% of standard metabolic rate [25] in animal cells (level reaches 70% in brain). NKA concentration in tissues varies significantly with around a 160,000-fold difference between the lowest (erythrocytes) and the highest (brain cortex) value. NKA has major contributions in brain, immune system, kidney, heart, skeletal muscles, vascular smooth muscles, erythrocytes etc. as described in [20].

The paper is organized as follows, we reconstitute NKA into GUVs of precisely controlled single-phase (l_o) and two-phase (l_o/l_d) membrane fluid phases. The measurements of protein activity and density in GUVs are discussed, followed by the investigation of the extent of water relaxation in the membrane in the active and non-active state of NKA. The spatial distribution and orientation of NKA is investigated at the single-molecule level in free-standing membranes by collapsing GUVs and rapidly immobilizing the collapsed membrane on a solid support. Unbinding of vesicle patches from the solid support is observed as a consequence of NKA activity. Finally, we discuss the implications of our work and possible adaptations of the method for other lipid–protein systems.

2. Materials and methods

1, 2-dioleoyl-sn-glycero-3-phosphocholine (DOPC), cholesterol and 1, 2-dipalmitoyl-sn-glycero-3-phosphocholine (DPPC) were purchased from Corden-Pharma. The fluorescence probes, N-Lissamine rhodamine B 1, 2-dihexadecanoyl-sn-glycero-3-phosphoethanolamine, triethylammonium salt (RhPE), and naphthopyrene (NaP) were purchased from Molecular Probes and Sigma, respectively. Chloroform was of HPLC grade quality purchased from Rathburn (Micro-lab, Aarhus, Denmark). 8.65 mM stock solutions in chloroform of each lipid are prepared separately. Glucose and sucrose were from Sigma, NaCl (sodium chloride, purity >99.5%) was from Fluka, whereas L-histidine (purity >99%) and $MgCl_2$ (magnesium dichloride, purity >99%) were from Sigma-Aldrich. Ultra-pure MilliQ water (18.3 MOhm cm) was used in all steps involving water. The osmolarity of solutions was checked using an osmometer (Osmomat 030, Gonotec GmbH, Berlin, Germany). Four types of buffers are prepared, buffer-A (200 mM sucrose, 30 mM NaCl, 30 mM histidine, 2 mM $MgCl_2$ at pH 7) and buffer-B (200 mM glucose, 30 mM NaCl, 30 mM histidine, 2 mM $MgCl_2$, buffer-C (200 mM sucrose, 30 mM NaCl, 30 mM histidine at pH 7) and buffer-D (200 mM glucose, 30 mM NaCl, 30 mM histidine) at pH 7. Na2ATP was purchased from SIGMA and a stock solution of 1 M was prepared. The pH of the Na2ATP was adjusted to 7.4 by adding 0.5 M TRIS.

2.1. Preparation of functional proteoliposomes

NKA purified from shark rectal glands was reconstituted into small unilamellar vesicles (SUVs) [24]. Essentially, NKA and the lipids, (a) DOPC and (b) DOPC-chol (60%–40%), were co-solubilized in 130 mM NaCl, 4 mM $MgCl_2$, and 30 mM histidine, pH 7.0 at a lipid/protein weight ratio of 10 using the nonionic detergent $C_{12}E_8$ (ethylene glycol dodecyl monoether) at 4 mg/mg protein. After equilibration the

detergent was removed by addition of hydrophobic Bio-Beads, and SUVs containing reconstituted NKA spontaneously formed. These proteoliposomes were unilamellar with a diameter of about 220 nm, as determined from freeze-fracture EM [19] and quasi-elastic laser light scattering [24]. The proteoliposomes are stored at -80°C for prolonged use. The ions transport properties of NKA in SUVs is measured using a probe namely "Oxonol" [26] whose fluorescence intensity is proportional to the amount of membrane potential that is created due to pumping of Na and K ions across the membrane. Briefly, the protein content of the proteoliposomes (and GUVs) was determined according to Petersons modification [27] of the Lowry method [28], and the specific hydrolytic activity of reconstituted NKA by the method of Baginski [29]. The orientation of reconstituted NKA was determined from functional tests benefitting from the sidedness of the NKA, as described in [30,24]. In proteoliposomes, typically, ~50% of the protein incorporated with an orientation as in the cell (r-o), ~15% with the opposite orientation (i-o), and the remaining ~35% with both sides exposed (n-o). The test medium for activity measurements contained 120 mM NaCl, 30 mM KCl, 4 mM $MgCl_2$, 3 mM ATP, and 30 mM histidine buffer pH 7.4. At these conditions only non-oriented (n-o) NKA is activated since the ATP substrate site of r-o oriented enzyme is shielded inside the GUVs, and the extracellular face of i-o oriented pumps is devoid of K^+ inside the GUVs, which contain 130 mM Na^+ and no K^+-ions.

2.2. Preparation of small unilamellar vesicles (SUVS)

The lipid mixtures are dissolved in chloroform of (i) 8.65 mM DOPC-chol (60%–40%) containing RhPE at 0.4 mol%, (ii) 8.65 mM DPPC-chol (53.8%–46.2%) containing RhPE and naphthopyrene (NaP) both at 0.4 mol%, (iii) 8.65 mM DPPC-chol (53.8%–46.2%) containing RhPE at 0.4 mol%, (iv) 8.65 mM DOPC-chol (60%–40%) containing the Laurdan at 4 mol%, (v) 8.65 mM DPPC-chol (53.8%–46.2%) and (vi) 8.65 mM DOPC containing RhPE at 0.4 mol%. Around 500 μL of the 8.65 mM lipid mixture solution is placed in a flask and chloroform is removed from sample by using a rotatory evaporator at 50°C for about an hour. The sample flask is kept in vacuum for about an hour to remove any residual chloroform at room temperature (23°C). 500 μL of milli-Q water is added to the flask to hydrate the lipids and is mixed using the rotatory evaporator without vacuum-tight conduit at 23°C (for DOPC-chol mixture) and 45°C (for DPPC-chol mixture), for about an hour. The hydrated lipid sample is transferred into an eppendorf, and 500 μL of milli-Q water is re-added to sample flask and mixed, resulting in an overall 1 ml volume of the 4.325 mM hydrated lipid sample. A tip-ultrasonicator (Misonixs 3000, Qsonica, Newtown, CT operating at frequency 20 kHz) is used to prepare SUVs of 1 ml each of the lipid solutions in water inside a glass vial kept in an ice-bath (to prevent heat-induced chemical degradation of lipids) in the following sequence: one step of sonication for 10 s and break for 5 s at 2 W power, for total sonication and break time of 20 min and 10 min respectively. In this way, we have prepared SUVs of concentration 4.325 mM in water of (a) DOPC-chol (60%–40%) containing RhPE, (b) DPPC-chol (53.8%–46.2%) containing RhPE and NaP, (c) DPPC-chol (53.8%–46.2%), (d) DOPC-chol (60%–40%) containing Laurdan, (e) DPPC-chol (53.8%–46.2%) containing RhPE and (f) DOPC containing RhPE, as listed in the Table 1. In case the SUVs have been stored at -20°C, we have ultrasonicated the SUVs with the same protocol as mentioned above followed by extrusion in the liquid phase, using a Nuclepore polycarbonate membrane filters with pore size of 100 nm.

2.3. Electroformation of GUVs

We have prepared GUVs by mixing SUVs suspensions (A and B, as listed in the Table 1), as described in [31]. A detailed description of the protocol explaining the NKA reconstitution in GUVs in minute details is described in [32] in physiological buffer and temperature conditions. We have prepared GUVs of eight samples (c.f. Table 1). The total protein/lipid molar ratio (n_P/n_L) and the number density (N) of the NKA in samples is calculated and is given in the Table 1 assuming the molecular weight of NKA as 147 kDa, the area of the pump and the lipid as 1134 $Å^2$ and 64 $Å^2$ respectively.

2.4. Confocal microscopy

For confocal microscopy, a Zeiss LSM 510 Meta confocal laser scanning fluorescence microscope (Carl Zeiss GmbH, Jena, Germany) is used. 100 μl of the GUVs suspension prepared in the buffer A were transferred to an eight-well microscopy chamber (Nunc Lab-Tek, Thermo Scientific, Waltham MA, USA) already filled with 1 ml of buffer B (see materials) at room temperature and imaged with a 40X, C-Apochromat, water immersion objective with NA = 1.2. Two-channel image stacks were acquired using multi-track mode, using Argon lasers of wavelengths 458 nm and 543 nm, for NaP and RhPE excitation, respectively. The lasers were directed to sample using two dichroic mirrors (HFT 458/514, HFT 488/543/633) for exciting NaP and RhPE respectively. Fluorescence emission was collected with photo-multiplier-tube (PMT) detectors. A beam splitter was used to eliminate remnant scattering from the laser sources (NFT 545) in a two-channel configuration. Additional filters were incorporated in front of the PMT detectors in the two different channels to measure the fluorescent intensity, i.e., a long-pass filter (>560 nm) for RhPE and a band-pass filter (500 ± 20) nm for NaP.

2.5. Epi-fluorescence and atomic force microscopy (AFM)

100 μl of the GUVs suspension prepared in the buffer C were transferred to a fluid cell (Biocell, JPK Instruments AG) filled with 1 ml of buffer D (see materials), with freshly cleaved mica glued on the round coverslips at room temperature. A Nikon TE2000 inverted microscope with 4X and 40X long working distance objective (Nikon ELWD, Plan Fluor, NA = 0.6) was used for epi-fluorescence observations combined with a JPK Nanowizard AFM system (JPK instruments AG). As appropriate for the RhPE probe, fluorescence excitation was done at 540 nm with a Xenon lamp (PolychromeV, Till Photonics GmbH, Grafeling, Germany) and a G-2a filter cube (Nikon) was used for imaging. Images were recorded with a high-sensitivity EMCCD camera (Sensicam em, 1004 × 1002 pixels, PCO-imaging, Kelheim, Germany) and operated with TILLvision software (Till Photonics GmbH). Epi-fluorescence

Table 1
Samples are prepared by mixing SUVs A and B.

Label	Lipid composition	(n_P/n_L) %	N	SUVs (A)	Proteoliposomes (B)
I	DOPC-chol (60%–40%), RhPE	0.019	302	DOPC-chol (60%–40%), RhPE	NKA, DOPC-chol (60%–40%)
II	DOPC-chol-DPPC (35%–30%–35%), RhPE, NaP	0.012	190	DPPC-chol (53.8%–46.2%), RhPE, NaP	NKA, DOPC
III	DOPC-chol (60%–40%)	0.038	603		NKA, DOPC-chol (60%–40%)
IV	DOPC-chol-DPPC (35%–30%–35%)	0.012	190	DPPC-chol (53.8%–46.2%)	NKA, DOPC
V	DOPC-chol (60%–40%), Laurdan	0.019	302	DOPC-chol (60%–40%), Laurdan	NKA, DOPC-chol (60%–40%)
VI	DOPC-chol (60%–40%), Laurdan	0	0	DOPC-chol (60%–40%), Laurdan	
VII	DOPC-chol-DPPC (35%–30%–35%), RhPE	0.012	190	DPPC-chol (53.8%–46.2%), RhPE	NKA, DOPC
VIII	DOPC-chol-DPPC (28%–39%–33%), RhPE	0.016	254	DPPC-chol (53.8%–46.2%), DOPC, RhPE	NKA, DOPC-chol (60%–40%)

(n_P/n_L) % is the ratio of the molar fraction of protein to lipids in samples and N is the number density of NKA/$μm^2$.

images were analyzed with ImageJ (National Institute of Health, USA). AFM is operated in the intermittent contact mode. Silicon cantilevers for soft-tapping are used (Nanosensors PPP-NCST-50), having a spring constant of 1.2–29 mN/m, with the AFM tip of thickness around 10–15 nm and a resonance frequency of 76–263 kHz. AFM images were processed and analyzed using the scanning probe image processor (SPIP, Image metrology, Hø rsholm, Denmark) and Mathematica (Wolfram Research).

2.6. Immunofluorescence labeling

For immunofluorescence labeling of pumps we have used Primary (PAb.) and secondary (SAb.) antibodies. Primary antibodies (PAbs) is a rabbit 55 kDa, C-terminal specific antibody that binds to anti-rabbit Secondary antibodies and is prepared by Prof. Cornelius. Secondary antibodies (SAbs) are tagged with Alexa Flour 488 purchased from Invitrogen (A11008). 100 μl of the GUVs suspension prepared in the buffer C of sample I were transferred to a fluid cell (Biocell, JPK Instruments AG) filled with 1 ml of buffer D (see materials), with freshly cleaved mica glued on the round coverslips at room temperature. Vesicle-patches of the GUVs were formed following the protocol described in [13] as described in the next paragraph. The patches are first incubated with PAbs at 23°C, overnight in the dark. Excess PAbs are washed with the buffer C and sample is incubated with SAbs for 2–3 h in the dark at 4°C. Excess SAbs are washed with the buffer C. The mica sheet is inverted in the observation chamber before fluorescence imaging. The fluorescence images are obtained using Leica TSC SP8 STED setup (Berlin, Germany) and excitation was done at 488 and 543 nm using a white light laser. The emission was recorded at 500–520 nm for SAbs and at 560–580 nm for RhPE using the gated hybrid detector (0.3 ns). Control experiments with GUVs of sample VI (containing no proteins) show no specific labeling of Abs with the membrane (the data is not shown).

2.7. Membrane-patch unbinding experiments

We transfer about 50 μl of the GUVs prepared in the buffer C of samples I and VIII in an fluid chamber containing osmotically matched buffer D. After most of the GUVs settle down on the mica substrate (~30–60 min), we add 1 μl of the concentrated $MgCl_2$-stock solution (final concentration 2 mM) to form the membrane-patches from GUVs, as described in [13]. 1 μl of the concentrated ATP solution was added in the observation chamber such that the final concentration of Mg^{+2}-ions is 2 mM.

2.8. Laurdan generalized polarization (GP) measurements

We transfer about 200 μL of the GUVs of samples V and VI prepared in the buffer A in an observation chamber containing 1 ml of an osmotically matched buffer B. Laurdan is an amphiphilic fluorescence probe whose fluorescence emission is sensitive to the dynamics of water molecules in the vicinity of its fluorescence moiety located at the lipid bilayer interface. If the extent of water relaxation around the probe increases (e.g., as in a gel-to-fluid phase transition), the maximum fluorescence emission intensity of Laurdan shifts from 440 nm to 490 nm [33]. LAURDAN GP measurements were performed on a custom-build microscope setup on a specially constructed Olympus IX70 microscope. The objective used was a 60X water objective with an NA of 1.2. The excitation light source was a femtosecond Ti:Sa laser (HP Mai Tai, tunable excitation range 690–960 nm, Spectra Physics, Mountain View, CA) and the excitation wavelength was 780 nm. The fluorescence signals were collected in two separate detectors (I_b and I_g); equipped with band-pass filters: 446 ± 23 nm and 492 ± 23 nm [34]. Likewise, LAURDAN GPs were calculated using the following equation: $GP_{ex} = (I_b - GI_g)/(I_b + GI_g)$. The correction factor G was calculated by acquiring GP images of a known LAURDAN reference solution (LAURDAN 2 μM in DMSO) in the microscope at the same instrumental conditions used in the GUVs experiments (for further details see [34]).

2.9. Voronoi analysis

We have analyzed the AFM topography images of the vesicle patches containing NKAs using the Voronoi analysis program in Mathematica (Wolfram Research). A Voronoi diagram shows partitioning of a plane with n points into convex polygons such that each polygon contains exactly one generating point which in our case is a protein (or a protein-cluster) and every point in a given polygon is closer to its generating point than to any other. A cumulative histogram of the specific-area of the Voronoi cells $t = (a/\bar{a})$ in a vesicle patch is used for finding the spatial distribution of the proteins in the membrane where a and $\bar{a}$ represent the area and the average area of the Voronoi cells respectively. An inverse of the area of the Voronoi cells in a vesicle patch gives the number of proteins per unit patch area or the number density of the proteins (N). The Delaunay triangulation is dual to the Voronoi diagram and gives information about the distance or the bond length (s) between any two proteins (or clusters). A histogram of s gives the nearest neighbor distance distribution.

3. Results

3.1. Reconstitution of NKA in two- and three-lipid-component GUVs

Confocal images of giant vesicles containing NKA, of sample I (Fig. 1c) and sample II (Fig. 1d) is shown. Vesicles are 5–50 μm in diameter and are prepared by mixing two populations of SUVs [32] in the buffer A and transferred in the buffer B for observations. We choose quasi-spherical GUVs for confocal scanning. We have also monitored the osmotic pressure of the system and do not find any changes in the osmotic pressure of the GUVs-suspension before and after the experiments. Fig. 1e shows a two-dimensional fluorescence intensity histogram for the surface of a typical GUV, which is used for precise segmentation of membrane phases [36] and quantifying the area-fraction of the l_o/l_d domains. The variation in the measured l_o area-fraction for a batch of vesicles (Fig. 1f) has a mean value of $A(l_o)/A$ being 0.57 ± 0.03 (mean ± SEM, N = 16). GUVs of the same composition that were produced from hydration of dried lipids mixed in organic solvent show similar value of $A(l_o)/A$ (c.f. color diagram in Fig. 1g). This suggests that the lipids in the membranes containing NKA are well mixed and that the vesicle sample is uniform.

3.2. Hydrolytic activity and density of the reconstituted NKA in GUVs

GUVs of samples III and IV are prepared for protein activity and density measurements in the buffer A, as described in [32]. The protein content in sample III and IV is measured and found to be almost 40% (241 pumps/μm^2) and 30% (50 pumps/μm^2) respectively, with respect to the initial proteoliposomes. The specific hydrolytic activity of reconstituted NKA in GUVs is estimated from the measured hydrolytic activity of NKA with a n-o orientation assuming that the fraction of enzyme with this orientation is preserved from the proteoliposomes, where it is measured to be 33%. The specific activity of sample III and IV is found to be 147 ± 2 μmol/mg h (mean ± SEM, n = 6) and below 10 ± 2 μmol/mg h (mean, n = 6), respectively, at 23°C. The activity for GUVs of sample III is about the same as in the proteoliposomes [30], whereas for ternary GUVs it was barely measurable. Thus, we found that the hydrolytic activity of NKA is membrane phase dependent and is not directly proportional to the protein density, which is consistent with the previous experimental observations [37] discussed in this paper.

3.3. Changes in the lipid bilayer hydration upon NKA reconstitution

We have calculated the Laurdan GP values in GUVs of samples V and VI before and after addition of the ATP and Fig. 1h shows the results. A GP value of 0.37 ± 0.005 (mean ± SEM, n = 35) is found in the absence of NKA, which corresponds to the extent of solvent relaxation observed for the l_o phase, as reported earlier [33]. Reconstitution of NKA results in a higher value of 0.43 ± 0.003 (mean ± SEM, n = 30). When NKA is turned active, we obtain a value 0.425 ± 0.002 (mean ± SEM, n = 73) similar to the non-active case. We have checked that the presence of ATP alone does not affect the GP value significantly.

3.4. Orientation and spatial distribution of the reconstituted NKA in vesicle patches

We have transferred individual GUVs of samples I and VII onto a mica support forming planar bilayer patches. Time-lapse data showing the single and two phase GUVs before and after the transfer is shown in Fig. 2. Single phase GUVs are settled at the bottom of the observation chamber (Fig. 2a), which upon adding Mg^{+2} ions form bilayer patches (Fig. 2b). Fig. 2c displays the membrane area (green) in the patches. Fig. 2d, e show the two-phase GUVs and the corresponding patches respectively for which the l_o and the l_d membrane phases are displayed schematically in Fig. 2f.

3.4.1. DOPC-chol (60%–40%)-NKA vesicle patches

Figs. 3a, b are the epi-fluorescence and AFM topography images, respectively, of a vesicle patch of sample I. Fig. 3b reveals many small-scale elevated particles embedded in the membrane. The phase-lag image (Fig. 3c) of the same patch shows that the particles appear dark, implying that they have different stiffness compared to the bilayer. A graphical representation of Fig. 3a showing the overall vesicle patch area in Fig. 3d. Fig. 3e is a scan of a small region of the patch revealing the spatial arrangement of the particles. We have investigated the height- and phase-contrast profile of two arbitrary selected particles showing vertical height of around z = 3–4 nm and a lateral extent around 50 nm (convoluted by the AFM-tip size) in Fig. 3f. The phase is reduced by ~1-2 degree compared to the flat bilayer. Fig. 3g is a color-coded three-dimensional height profile of the same particles (Fig. 3e), where different colors indicate different z-height levels varying between −3.6 nm to 1.2 nm. We have analyzed 170 particles in different vesicle patches. In Fig. 3h, the two distinct populations of particle heights around 2 nm and 4 nm with equal occurrence in the vesicle patch are clearly seen. We have plotted the histogram of the number density (N) of the particles as shown in Fig. 3i and found N ~$100/\mu m^2$ resulting in a mean distance between any two particles to be around 100 nm, assuming a homogeneous spatial distribution. Fig. 3j is the cumulative histogram of the Voronoi specific area, $t = (a/\bar{a})$, of the particles to which we fit $f(t) = c\int_0^t x^{(\lambda-1)}e^{-\eta x}dx$, where the fitting parameters are $\lambda = \eta = 3.61$ and $c = \eta^{\lambda}/\Gamma(\lambda)$ as found [38] for a random distribution.

In the section 3.2, we have measured the protein density in sample III and found that 40% of the total protein content present initially in the proteoliposomes gets reconstituted into GUVs. From this we have estimated the protein density and obtain N ~$121/\mu m^2$ for sample I. This implies a mean distance between two particles in the bilayer corresponding to ~ 90 nm for a homogeneous distribution. Thus the density of particles in the vesicle patches is consistent with the density determined from biochemical assays.

Fig. 4a, b shows an antibody labeled vesicle patch in which the presence of the reconstituted proteins is confirmed by immunolabeling. Further, the epi-fluorescence images of vesicle patches on mica in the absence (Fig. 4c) and presence (Fig. 4d) of ATP show that the patches spontaneously unbind from the substrate, as these are no longer visible in the epi-fluorescence microscope. Figs. 4e, f show the epi-fluorescence images of many patches after adding the ATP on a larger spatial scale for the vesicle patches of samples I (Fig. 4e) and VIII (Fig. 4f). Experiments on ternary-mixture vesicle patches containing NKA (Fig. 4f) and binary-mixture vesicle patches without NKA to which ATP is added do not unbind. We have investigated the ternary-mixture vesicle patches containing NKA in detail and will be described in the section 3.4.2.

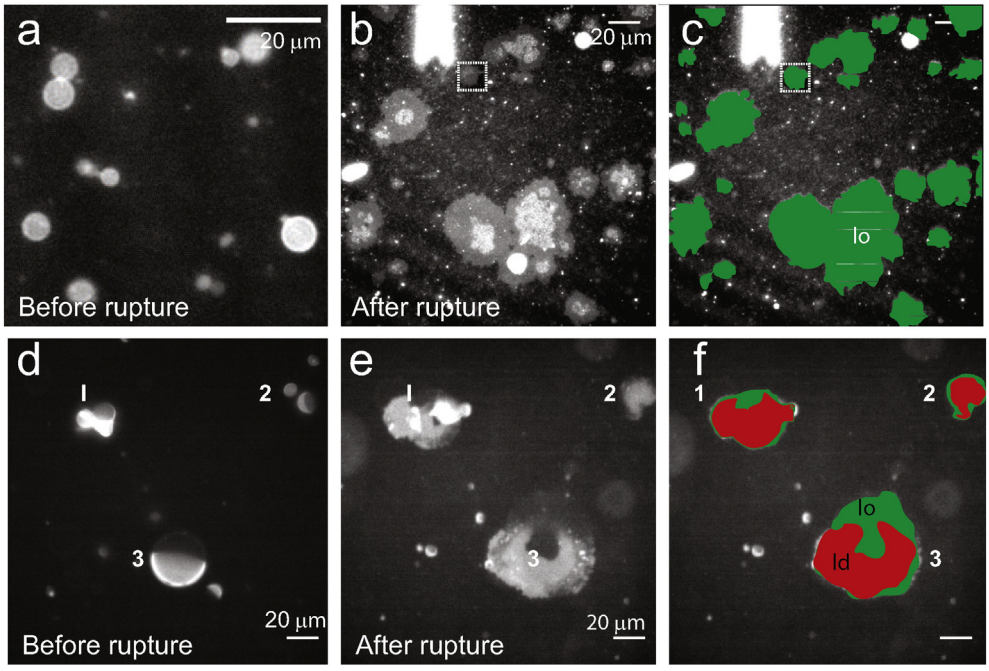

Fig. 2. Epi-fluorescence images of the collapse of GUVs on mica. (a) Epi-fluorescence image of GUV of sample I (containing NKA) settled on a mica support. (b) Vesicle patches formed after GUVs collapse. A white box denotes a patch that is selected and scanned with AFM (Fig. 3a). (c) A graphical representation of the vesicles patches (in b). Green indicates the membrane surface in the l_o phase. (d) Epi-fluorescence image of GUVs of sample VII. The bright and dark regions are the l_d and l_o membrane phases, respectively. (e) Vesicle patches formed after GUVs collapse. 1–3 represent the same GUVs as in (d), after the collapse. (f) A graphical representation of the vesicles patches shown (in e) highlighting l_d (red) and l_o (green) domains.

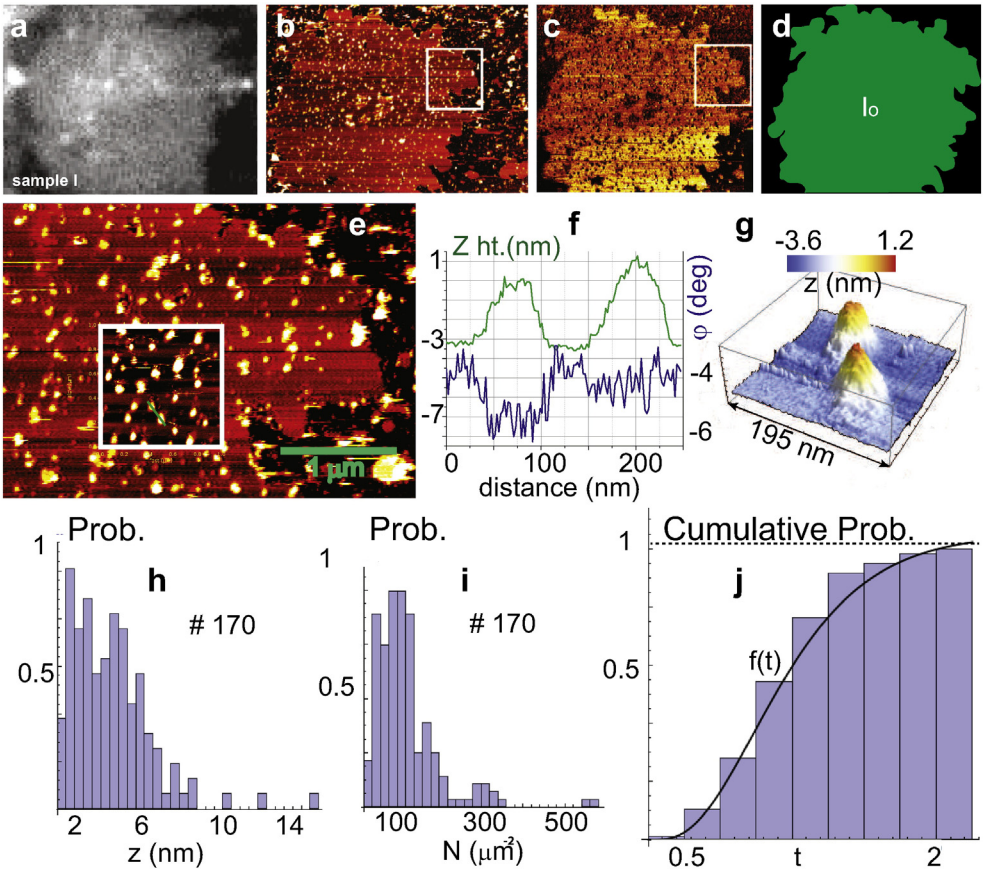

Fig. 3. Images of nanoscopic distribution of NKA in the l_o membrane phase vesicle patches. (a) Epi-fluorescence image of a vesicle (sample I) patch. (b, c) AFM topography and phase-contrast images of the same vesicle patch. (d) A cartoon of the vesicles patch with green color indicating the membrane surface that is in the l_o phase. (e) High-pixel resolution AFM topography image of the patch region selected in the white box in (b). (f) Height (z, green-color) and phase (ϕ, blue-color) line profiles along the cut line (within the white box in e). (g) Three-dimensional view of the same two particles (as in f) inside the white box in (e) with a color-code representation of the height deformation. (h) Histogram of the z-height (nm) and the (i) number-density (N in μm^{-2}) of the 170 arbitrary particles in different patches. (j) Cumulative distribution function of the Voronoi cells specific area $t = (a/\overline{a})$, where a and $\overline{a}$ is the area and average area of the Voronoi cells respectively. The solid black line shows a fit $f(t)$ to a random distribution of the normalized specific areas (t).

3.4.2. DOPC-DPPC-chol(35%–35%–30%)-NKA vesicle patches

GUVs of sample VII are prepared and vesicle patches are formed as described above. We select one arbitrary vesicle patch (Fig. 5a), for which the AFM topography image is shown in Fig. 5b. Fig. 5c is a graphical illustration of Figs. 5a, b highlighting the l_o and the l_d membrane phases. Fig. 5d is an AFM topography image of a scanned region in the patch close to the macroscopic l_o/l_d domain boundary (shown in Figs. 5a and 5c). Fig. 5e is drawn to highlight the l_o/l_d domains by graphical illustration of Fig. 5d. Fig. 5f shows a height profile taken in Fig. 5d confirming the presence of l_d membrane phase fluctuations inside the macroscopic l_o domain with a step height difference of 0.9 nm. The image also reveals that the intra-membrane particles are heterogeneously distributed in a complex interplay with the l_o/l_d domains. A high resolution AFM topography scan of a selected region in the vesicle patch as shown in the Fig. 6a reveals that elevated particles greatly vary in size. Figs. 6b, c are the Voronoi diagram and the Delaunay triangulation respectively for the particles present in the same patch. A nearest-neighbor particle distance distribution (s) for this patch reveals large variation in s. (See Fig. 6d.)

Fig. 7a shows an AFM topography scan of a vesicle patch showing many interfaces and elevated particles. A region in the Fig. 7a is selected (shown by a blue ellipse) of which a three-dimensional height profile (Fig. 7b) and two-dimensional height-projection contours (Fig. 7c) of one of the selected particles is shown, where height levels are varying between −1 nm and 5.4 nm (indicated by different colors). To quantify the membrane phases surrounding a particle, we calculate the area occupied by the particle and derive an equivalent circular area of radius r. The area-fraction of the l_d membrane phase within the circle of radius $R = \sqrt{2}\,r$ is calculated by counting the number of pixels in the AFM topography image leading to a vertical height decrease of 0.9 nm relative to the l_o membrane phase ($z = 0$) as shown in the Figs. 7b, c, i.e., similar to that of an l_o-l_d domains interface. Fig. 7d displays the height profiles taken in Fig. 7a revealing coexisting l_o/l_d domains. Figs. 7e, f show the height and the l_d membrane phase area-fraction $A(l_d)/A$, respectively, for the 103 particles. Distinct populations of particles of height around 1–3 nm, 4–6 nm, and 6–8 nm are found to protrude out from the lipid bilayer (Fig. 7e). Fig. 7f shows the the area-fraction of the l_d membrane phase in the vicinity of 103 particles suggesting that $A(l_d)/A$ has a broad distribution and the particles are indeed located at the l_o/l_d interface.

As described previously (Fig. 4f), we have also studied these vesicle patches in order to see possible unbinding effects due to activity in the presence of ATP but found that the patches do not unbind. We suggest that this is due to the very low NKA activity in the ternary systems, as measured here and also reported earlier [39], attributed mainly to the interfacial localization of NKA as will be discussed further.

To summarize this section, we have found that the elevated particles of height 1–3 nm and 4–6 nm are found to be randomly distributed in a bilayer in the l_o phase, while these are clustered in the l_o/l_d coexisting domains and preferentially localized at the l_o/l_d domain boundaries. For data analysis we choose the particles or clusters locally and analyze each one of them individually to gather the detailed statistics, which is a major undertaking with the current technique. Figs. 3h, i, j show the z-

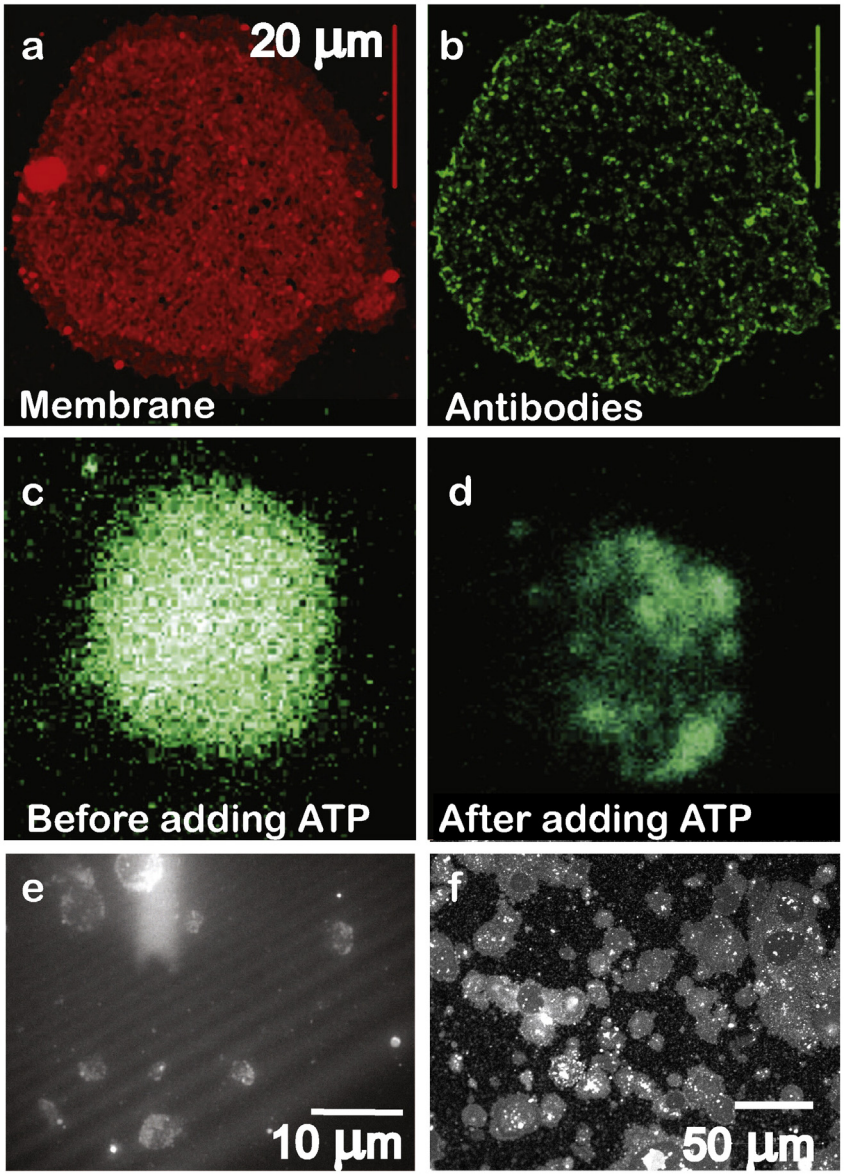

Fig. 4. Immunolabeling of NKA in a vesicle patch and unbinding of patch due to NKA activity. (a) Fluorescence image of an arbitrary selected vesicle patch (sample I) where red color indicates the membrane surface labelled by the RhPE dye. (b) The same patch (as in a) is shown after incubation with NKA-specific antibodies. The green color derives from Alexa-488 antibodies that specifically attach to the NKA. (c, d) Epi-fluorescence images of a single-phase vesicle patche (without antibodies) before (in c) and after (in d) the addition of ATP. (e, f) Epi-fluorescence images of many vesicle patches (without antibodies) after the addition of ATP, for samples I (in e) and VIII (in f).

height, particle density and cumulative spatial distribution data statistics for the 170 different particles respectively in vesicle patches of single phase membrane. For vesicle patches of two phase membrane, Fig. 7a shows many l_o/l_d interfaces and small clusters. We have made detailed quantifications of the z-height and membrane phase state surrounding the 103 clusters as shown in Figs. 7e, f respectively . From the density of particles (Fig. 3i, 100/μm^2), which is similar to the measured density of NKA (121/μm^2), and from the height histogram of the particles in the binary (Fig. 3h) and ternary (Fig. 7e) vesicle patches, we would therefore suggest that the particles of height 1–3 nm protruding from the bilayer correspond to i-o orientation of NKA, and those of height 4–6 nm correspond to the r-o orientation of NKA. If n-o pumps represent externally adsorbed protein, which is not integral in the bilayer, we would expect a height of less than 4 nm from the crystal structures and they may therefore be included in the particles of heights 1–3 nm. This would also be in accordance with the distribution of orientations measured from functional tests where r-o oriented NKA comprised about 50% of the protein [30].

4. Discussion and conclusions

We have studied the function and spatial distribution of NKA and how it is influenced by the lipid composition and the physical state of model membranes. Our main finding is that the hydrolytic activity of NKA is measured and found to be membrane phase-dependent and related to the lipid-domain structure of the membrane. We have also measured a significant change in the membrane hydration (GP data) due to the presence of non-active proteins. Our work suggests that NKA stabilizes the l_o/l_d domain interfaces by inter-domain localization. The l_o/l_d interfacial localization of NKA is also supported by structural data, which show distinct differences in the hydrophobic thickness at the membrane-spanning region [21,37].

It is well established that a determining factor for the solubility of integral proteins in fluid membranes is hydrophobic matching, i.e.; the length of the hydrophobic core of the TM domain of NKA (containing non-polar residues) should closely match the hydrophobic thickness of the lipid bilayer in order not to expose non-polar residues to water

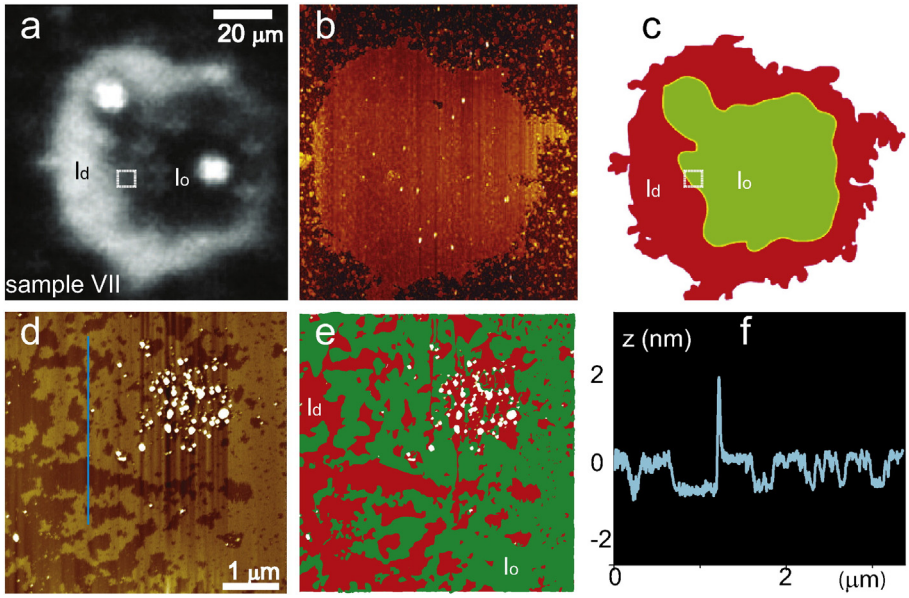

Fig. 5. Images of nanoscopic distribution of NKA in the l_o/l_d phase-coexistence region of vesicle patches (a) epi-fluorescence image of a vesicle patch (sample VII). In the l_o/l_d coexistence region, the l_d phase (bright region) of the membrane is labelled by the RhPE dye and the l_o phase (dark region) contains no dye. (b) AFM topography image of the same vesicle patch. (c) A cartoon of the vesicles patch (in b) with l_d (red) and l_o (green) domains. (d) High-pixel resolution AFM topography image of a region in the vesicle patch (shown by the white box in a and c). (e) A cartoon of the patch region (in d) with l_d (red) and l_o (green) domains. (f) Height line profile (along the blue-color line shown in d) displaying the l_d and l_o domains coexisting in the membrane with a difference in the z-height of around 0.9 nm.

[40,41,42,43]. Andersen and Koeppe [44] have shown by molecular dynamics simulation of Ca^{+2}-ATPase that hydrophobic mismatch induces local deformations in the lipid bilayer. Mutual adaptation of the protein to the bilayer by small rearrangements of amino acid side chains and α-helix tilts has also been suggested in [45]. In SERCA1a, E_1–E_2 conformational change of the NKA during turnover is followed by a change in the

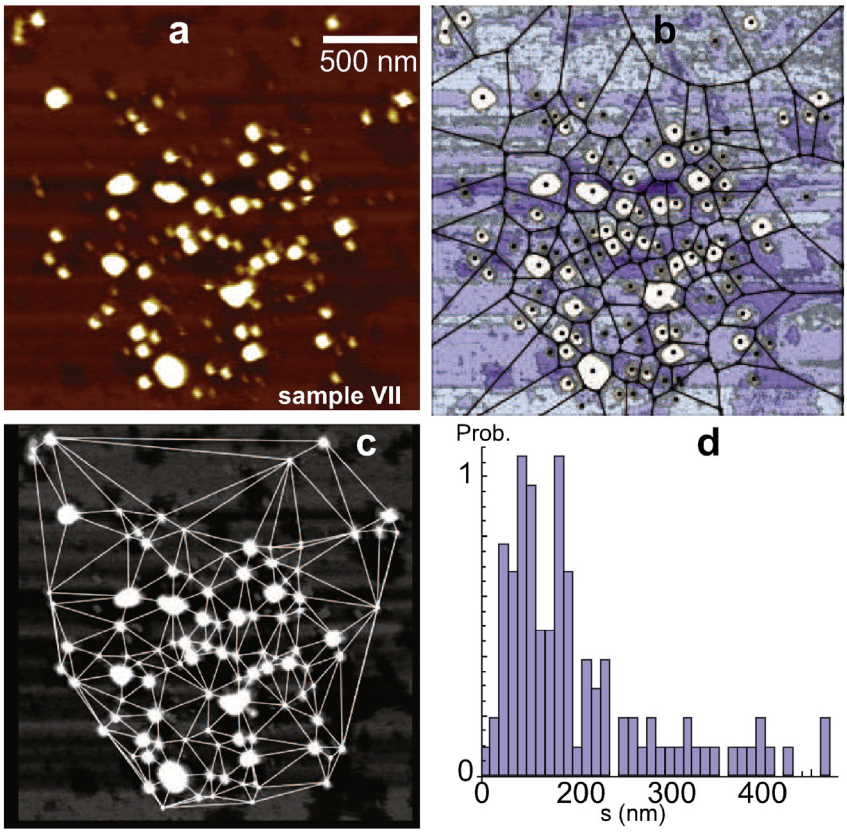

Fig. 6. Voronoi analysis of vesicle patches containing NKA. (a) AFM topography image of a vesicle patch containing NKA (sample VII). The bright regions are the elevated particles. (b) A Voronoi diagram indicating that particles have different sizes in the form of clusters. The black dot shows the centroid of the particles and white region shows the lateral extent of particles. (c) The Delaunay triangulation shows the proximity information or the bond length (s) between the two particles (or clusters). (d) Nearest-neighbor particle distance (s) distribution plot indicating particles are heterogeneously distributed.

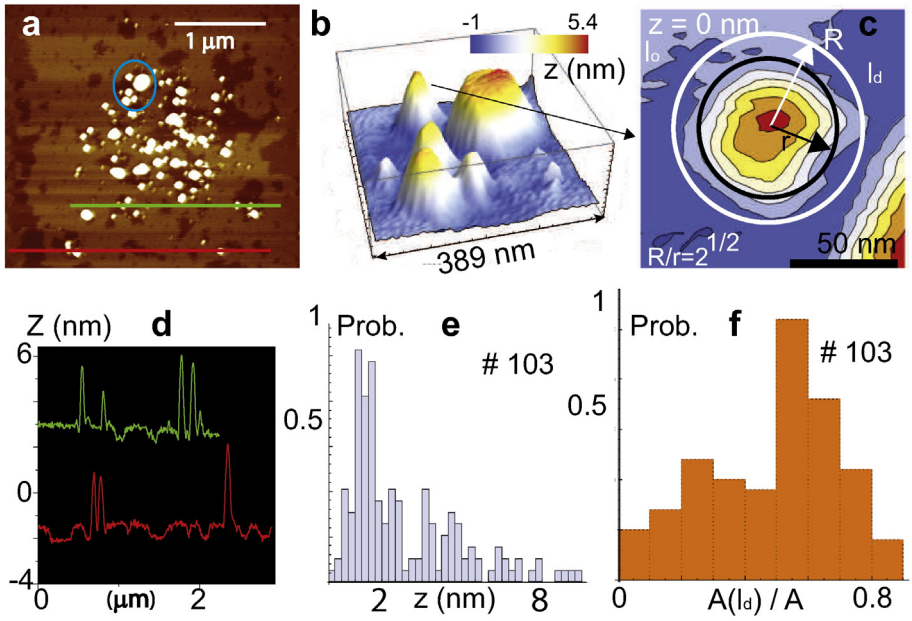

Fig. 7. Images of interfacial localization of NKA at the l_o/l_d domain boundaries and clustering effect. (a) AFM topography image of a selected region in a vesicle patch (sample VII). (b) Three-dimensional view of features (inside the blue ellipse in a) with a color-coded z-height scale . (c) Two-dimensional height-projection contours of a selected feature (in b pointed by an arrow) with the same color scale (as in b). z = 0 corresponds to the l_o membrane phase. R and r are radii of the two circles where $R = \sqrt{2}$ r. (d) Z-height line profile (in a) displaying the l_o and l_d domains with a step height difference of around 0.9 nm. (e) Histogram of the z-height for the 103 arbitrary selected particles. (f) Histogram of the area-fraction of the l_d phase A(l_d)/A in the vicinity of the 103 particles embedded in the membrane.

membrane thickness and residues interacting with phospholipids (PL) head groups, and the orientation of the whole protein. This would result in large changes in cross-sectional area of the TM region and lateral pressure profile of the lipid bilayer containing the pump. Experimentally, a significant shift in the NKA conformations has been shown previously by increasing the amount of cholesterol in the bilayer [46,19]. Thus the mixed solubility of NKA with respect to the l_o and l_d phases may favor an interfacial location.

A lower activity of NKA has previously been reported in the case where NKA is reconstituted into proteoliposomes with poly-unsaturated lipids (PUFA) [37]. It was suggested in [37] that a lower hydrolytic activity would result if the NKA localize at the two-phase domain boundaries instead of either of the phases; a hypothesis which we have examined in this paper. A similar conclusion was reached by Powalska et al. [47] who measured the GP values in vesicles with one (DMPC, DOPC) and two (DOPE-DOPC) lipid components in the l_d phase containing 1–3 mol% NKA, and found a higher Laurdan GP value, ΔGP ~ 0.35, in comparison with vesicles containing no NKA. Earlier, Bouvaris et al. have measured an increase in the membrane bending rigidity by 3.5 k_BT upon NKA reconstitution into the GUVs of sample III and found a decrease by 7 k_BT when NKA is activated by adding ATP [48]. We surmise that the mechanism behind this membrane softening and the resulting unbinding phenomenon is due to a conformational change of the protein during the pumping cycle [19].

A striking observation is the highly inhomogeneous distribution of NKA in the ternary mixtures, where the NKA is found primarily to be located in clusters associated with l_o and l_d microdomains (Figs. 6 and 7). Furthermore the clusters are located at the interfacial region between the macroscopic l_o and l_d phases (Fig. 7f). A possible explanation of this is that NKA is emulsifying the l_o/l_d phase coexistence, where the observed protein-rich cluster form a microemulsion droplet. This type of phenomenon is well known in standard oil–water surfactant systems [49]. Two-dimensional microemulsions stabilized by proteins may be a natural way to stabilize microdomains of l_o and l_d phases. Opposite to the recently suggested mechanism for formation of microdomains by quenched disorder in the lipid cooperativity, e.g., facilitated by proteins coupled to the cytoskeleton [6,7], microemulsion formation does not require external coupling to the membrane components.

Functional and structural observations on membrane bound NKA have indicated direct and specific interactions of phospholipids (PLs) and cholesterol to be responsible for both the stability and molecular activity of NKA [19,50,51]. The PL composition in shark enzyme preparation has the main fatty acids — 16:0, 18:1, 20:4 and 22:6 acyl chains [39]. In pig kidney enzyme preparations 18:0/18:1 PL is the best to support activity and 16:0 PC is one of the worst [21]. For this purpose, we have reconstituted the NKA in GUVs of DOPC (18:1 PL) and cholesterol containing vesicles in order to have fully active NKA. We expect that our studies will lead to further quantitative scrutiny of the presence of lipid-mediated heterogeneity in biological membranes. Immediate applications pertain to studies involving NKA and could involve other P-type ion-motive ATPase, such as Ca^{+2}-ATPase and H^{+}-ATPase, which are very similar to NKA in topology and molecular organization and furthermore are targets for cardiac drugs and disease-causing mutations.

Transparency document

The Transparency document associated with this article can found, in online version.

Acknowledgments

We thank the Danish Council for Independent Research | Natural Sciences (FNU), grant number 95-305-23443 (to OGM) for financial support and DAMBIC (Danish Molecular Bio-Imaging Center). TB thanks Prof. Derek Marsh (Max Planck Institute for Biophysical Chemistry, Gottingen, Germany) for very helpful discussions and DAMBIC (Danish Molecular Bio-Imaging Center) for access to equipment. We thank Bianca Franchi and Hanne Kidmose (Department of Biomedicine, Aarhus University, Denmark) for technical help with protein activity and protein density measurements. There are no conflicts of interests.

References

[1] L.A. Bagatolli, J.H. Ipsen, A.C. Simonsen, O.G. Mouritsen, An outlook on organization of lipids in membranes, searching for a realistic connection with the organization of biological membranes, Prog. Lipid Res. 49 (2010) 378–389.

[2] K. Simons, J.L. Sampaio, Membrane organization and lipid rafts, Cold Spring Harb. Perspect. Biol. 3 (2011) a004697.

[3] D. Lingwood, K. Simons, Lipid rafts as a membrane organizing principle, Science 327 (2010) 46–50.

[4] C. Eggeling, C. Ringemann, R. Medda, G. Schwarzmann, K. Sandhoff, S. Polyakova, V.N. Belov, B. Hein, C. Middendorff, A. Schönle, S.W. Hell, Direct Observation of the Nanoscale Dynamics of Membrane Lipids in a Living Cell, Vol. 4572009 1159–1162.

[5] J. Adler, A.I. Shevchuk, P. Noval, Y.E. Korchev, I. Parmryd, Plasma membrane topography and interpretation of single-particle tracks, Nat. Methods 7 (2010) 170–171.

[6] S. Arumugam, E.P. Petrov, P. Schwille, Cytoskeletal pinning controls phase separation in multicomponent lipid membranes, Biophysical J. 108 (2015) 1104–1113.

[7] R. Raghupathy, A.A. Anilkumar, A. Polley, P.P. Singh, M. Yadav, C. Johnson, S. Suryawanshi, V. Saikam, S.D. Sawant, A. Panda, Z. Guo, R.A. Vishwakarma, M. Rao, S. Mayor, Transbilayer lipid interactions mediate nanoclustering of lipid anchored proteins, Cell 161 (2015) 581–594.

[8] J.H. Ipsen, K. Jørgensen, O.G. Mouritsen, Density fluctuations in saturated phospholipid bilayers increase as the acyl chain length decreases, Biophysical J. 58 (1990) 1099–1107.

[9] M. Morrow, D. Singh, D. Lu, C.W. Grant, Glycosphingolipid fatty-acid arrangement in phospholipid bilayers-cholesterol effects, Biophysical J. 68 (1995) 179–186.

[10] M.C. Rheinstädter, J. Das, E.J. Flenner, B. Brüning, T. Seydel, I. Kosztin, Motional coherence in fluid phospholipid membranes, Phys. Rev. Lett. 101 (2008) 248106.

[11] C.L. Armstrong, D. Marquardt, H. Dies, N. Kučerka, Z. Yamani, T.A. Harroun, J. Katsaras, A. Shi, M.C. Rheinstädter, The observation of highly ordered domains in membranes with cholesterol, PLoS One 8 (2013), e66162.

[12] A.R. Honerkamp-Smith, P. Cicutta, M.D. Collins, S. Veatch, M. Nijs, M. Schick, S. Keller, Line tensions correlation lengths and critical exponents in lipid membranes near critical points, Biophysical J. 95 (2008) 236–246.

[13] T. Bhatia, P. Husen, J.H. Ipsen, L.A. Bagatolli, A.C. Simonsen, Fluid domain patterns in free-standing membranes captured on a solid support, Biochim. Biophys. Acta Biomembr. 1838 (2014) 2503–2510.

[14] T. Gil, J.H. Ipsen, O.G. Mouritsen, M.C. Sabra, M.M. Sperotto, M.J. Zuckermann, Theoretical analysis of protein organization in lipid membranes, Biochim. Biophys. Acta 1376 (1998) 245.

[15] T. Hønger, K. Mortensen, J.H. Ipsen, J. Lemmich, R. Bauer, O.G. Mouritsen, Anomalous swelling of multilamellar lipid bilayers in the transition region by renormalization of curvature elasticity, Phys. Rev. Lett. 72 (1994) 3911–3914.

[16] L. Cruzeiro-Hansson, J.H. Ipsen, O.G. Mouritsen, Intrinsic molecules in lipid-membranes change the lipid-domain interfacial area, cholesterol at domain interfaces, Biochim. Biophys. Acta 979 (1989) 166–176.

[17] J. Skou, The influence of some cations on an adenosine triphosphatase from peripheral nerves, Biochim. Biophys. Acta 23 (1957) 394–401.

[18] Z. Xie, Molecular mechanisms of nak-atpase mediated signal transduction, Ann. N. Y. Acs. Sci. 986 (2003) 497–503.

[19] F. Cornelius, Functional reconstitution of the sodium pump, kinetics of exchange reactions performed by reconstituted Na^+,K^+-ATPase, Biochim. Biophys. Acta Biomembr. 1071 (1991) 19–66.

[20] B. M. Anner, Na^+,K^+-ATPase, 2015.

[21] F. Cornelius, M. Habeck, R. Kanai, C. Toyoshima, S.J.D. Karlish, General and specific lipid–protein interactions in Na^+,K^+-ATPase, Biochim. Biophys. Acta 1848 (2015) 1729–1743.

[22] R. Kanai, H. Ogawa, B. Vilsen, F. Cornelius, C. Toyoshima, Crystal structure of a Na^+-bound Na^+,K^+-ATPase preceding the E1-P state, Nature 502 (2013) 201–206.

[23] T. Shinoda, H. Ogawa, F. Cornelius, C. Toyoshima, Crystal structure of the sodium-potassium pump at 2.4 Å resolution, Nature 459 (2009) 446–450.

[24] F. Cornelius, J.V. Møller, Liposomes in Reconstitution of Ion-Pumps. Handbook of Non-Medical Applications of Liposomes, vol. 2CRC press, Boca Racon FL, 1995.

[25] D.F. Rolfe, G.C. Brown, Cellular energy utilization and molecular origin of standard metabolic rate in mammals, Physiol. Rev. 77 (1997) 731–758.

[26] H.J. Apell, B. Bersch, Oxonol VI as an optical indicator for membrane potentials in lipid vesicles, Biochim. Biophys. Acta Biomembr. 903 (3) (1987) 480–494.

[27] G.L. Peterson, A simplification of the protein assay method of lowry et al. which is more generally applicable, Anal. Biochem. 83 (1977) 346–356.

[28] O.H. Lowry, Protein measurement with the folin phenol reagent, J. Biol. Chem. 193 (1951) 265–275.

[29] E.S. Baginski, P.P. Foa, B. Zak, Microdetermination of inorganic phosphate, phospholipids, and total phosphate in biologic materials, Clin. Chim. 13 (1967) 326–332.

[30] F. Cornelius, Incorporation of $C_{12}E_8$-solubilized Na^+,K^+-ATPase into liposomes: determination of sidedness and orientation, Methods Enzymol. 156 (1988) 156–167.

[31] T. Bhatia, P. Husen, J. Brewer, L.A. Bagatolli, P.L. Hansen, J.H. Ipsen, O.G. Mouritsen, Preparing giant unilamellar vesicles (guvs) of complex lipid mixtures on demand, mixing small unilamellar vesicles of compositionally heterogeneous mixtures, Biochim. Biophys. Acta Biomembr. 1848 (2015) 3175–3180.

[32] T. Bhatia, F. Cornelius, O. G. Mouritsen, J. H. Ipsen, Reconstitution of transmembrane protein Na^+,K^+-ATPase in giant unilamellar vesicles of lipid mixtures involving PSM, DOPC, DPPC and cholesterol at physiological buffer and temperature conditions, Nature Protocol/Protocol exchange doi:10.1038/protex.2016.010.

[33] L.A. Bagatolli, Fluorescent Methods to Study Biological Membranes, vol. 13Springer, Heidelberg, 2013.

[34] J. Brewer, J.B. Serna, K. Wagner, L.A. Bagatolli, Multiphoton excitation fluorescence microscopy in planar membrane systems, Biochim. Biophys. Acta 1798 (2010) 1301–1308.

[35] S. Veatch, I.V. Polozov, K. Gawrisch, S. Keller, Liquid domains in vesicles investigated by NMR and fluorescence microscopy, Biophysical J. 86 (2004) 2910–2922.

[36] P. Husen, L.A. Arriaga, F. Monroy, J.H. Ipsen, L.A. Bagatolli, Morphometric image analysis of giant vesicles: a new tool for quantitative thermodynamics studies of phase separation in lipid membranes, Biophys. J. 103 (2012) 2304–2310.

[37] F. Cornelius, N. Turner, H.Z. Christensen, Modulation of Na^+,K^+-ATPase by phospholipids and cholesterol: II. steady-state and presteady-state kinetics, Biochemistry 42 (2003) 8541–8549.

[38] F. Jarai-Szabo, Z. Neda, On the size distribution of Poisson Voronoi cells, Physica A 385 (2007) 518–526.

[39] F. Cornelius, Cholesterol dependent interaction of polyunsaturated phospholipids with Na^+,K^+-ATPase, Biochemistry 47 (6) (2008) 1652–1658.

[40] O.G. Mouritsen, M. Bloom, Mattress model of lipid–protein interactions in membranes, Biophysical J. 46 (1984) 141–153.

[41] M.O. Jensen, O.G. Mouritsen, Lipids do influence protein function — the hydrophobic matching hypothesis revisited, Biochim. Biophys. Acta 1666 (2004) 205–226.

[42] O.G. Mouritsen, Comprehensive Biophysics Membranes, vol. 5Academic Press, Oxford, 2012.

[43] D. Marsh, Energetics of hydrophobic matching in lipid–protein interactions, Biophysical J. 94 (2008) 3996–4013.

[44] O.S. Andersen, R.E. Koeppe, Bilayer thickness and membrane protein function: an energetic perspective, Annu. Rev. Biophys. Biomol. Struct. 36 (2007) 107–130.

[45] Y. Sonntag, M. Musgaard, C. Olesen, B. Schiøtt, J.V. Møller, P. Nissen, L. Thøgersen, Mutual adaptation of a membrane protein and its lipid bilayer during conformational changes, Nat. Commun. 2 (2011) 304.

[46] S. Yoda, A. Yoda, Phosphorylated intermediates of na,k-atpase proteoliposomes controlled by bilayer cholesterol, J. Biol. Chem. 262 (1987) 103–109.

[47] E. Powalska, S. Janosch, E. Kinne-Saffran, R.K. Kinne, C.F. Fontes, J.A. Mignaco, R. Winter, Fluorescence spectroscopic studies of pressure effects on nak-atpase reconstituted into phospholipid bilayers and model raft mixtures, Biochemistry 46 (2007) 1672–1683.

[48] H. Bouvrais, F. Cornelius, J.H. Ipsen, O.G. Mouritsen, Intrinsic reaction-cycle time scale of Na^+,K^+-ATPase manifests itself in the lipid–protein interactions of non-equilibrium membranes, Proc. Natl. Acad. Sci. 109 (2012) 18442–18446.

[49] S. Safran, Micelles Membranes Microemulsions and Monolayers, Springer, New York, 1994.

[50] M. Habeck, H. Haviv, A. Katz, E.K. Pardes, S. Ayciriex, A. Shevchenko, H. Ogawa, C. Toyoshima, S.J.D. Karlish, Stimulation inhibition or stabilization of Na^+,K^+-ATPase caused by specific lipid interactions at distinct sites, J. Biol. Chem. 290 (2015) 4829–4842.

[51] H. Haviv, M. Habeck, R. Kanai, C. Toyoshima, S.J.D. Karlish, Neutral phospholipids stimulate Na^+,K^+-ATPase activity a specific lipid–protein interaction, J. Biol. Chem. 288 (2013) 10073–10081.